

# POSSIBLE PHOTOMETRIC SIGNATURES OF MODERATELY ADVANCED CIVILIZATIONS: THE CLARKE EXOBELT

HECTOR SOCAS-NAVARRO<sup>1,2</sup>

<sup>1</sup>*Instituto de Astrofísica de Canarias, Avda Vía Láctea S/N, La Laguna, 38205, Tenerife, Spain*

<sup>2</sup>*Departamento de Astrofísica, Universidad de La Laguna, La Laguna, 38205, Tenerife, Spain*

(Received ; Revised ; Accepted )

Submitted to ApJ

## ABSTRACT

This paper puts forward a possible new indicator for the presence of moderately advanced civilizations on transiting exoplanets. The idea is to examine the region of space around a planet where potential geostationary or geosynchronous satellites would orbit (hereafter, the Clarke exobelt). Civilizations with a high density of devices and/or space junk in that region, but otherwise similar to ours in terms of space technology (our working definition of “moderately advanced”), may leave a noticeable imprint on the light curve of the parent star. The main contribution to such signature comes from the exobelt edge, where its opacity is maximum due to geometrical projection. Numerical simulations have been conducted for a variety of possible scenarios. In some cases, a Clarke exobelt with a fractional face-on opacity of  $\sim 10^{-4}$  would be easily observable with existing instrumentation. Simulations of Clarke exobelts and natural rings are used to quantify how they can be distinguished by their light curve.

*Keywords:* extraterrestrial intelligence — planets and satellites: detection — planets and satellites: terrestrial planets

## 1. INTRODUCTION

The discovery of thousands of exoplanets in recent years has sparked a surge of research on potential atmospheric biomarkers (see e.g., the recent reviews by [Schwieterman et al. 2017](#); [Grenfell 2017](#) and references therein). Future giant telescopes, such as the JWST, GMT, E-ELT or TMT, are expected to provide detailed analyses of the atmospheric composition of transiting exoplanets ([Hecht 2016](#); [Seager et al. 2009](#); [Angel et al. 2006](#); [Quanz 2015](#); [Wright et al. 2014c](#)). For the first time in history, humankind would be in a position to search for direct unequivocal evidence of life on planets around other stars.

While searching for exolife is starting to appear as a feasible endeavor, the search for intelligent life, or even technological civilizations, seems almost completely hopeless except under very specific circumstances. The main problem is the lack of suitable “technomarkers” (also referred to as technosignatures, [Schneider et al. 2010](#)), indicators that, analogously to the biomarkers, would unequivocally reveal the presence of technology.

Existing proposals in the literature for observable technomarkers are of extremely speculative nature. [Lingam & Loeb \(2017\)](#) analyze the possibility that the enigmatic fast radio bursts might be the propulsion system of an advanced interstellar form of transportation. [Forgan & Elvis \(2011\)](#) put forward that depletion of certain metallic elements in a stellar debris disk could be a sign of extensive asteroid mining by an advanced space-faring civilization. [Harris \(2002\)](#) used data from the Compton Gamma Ray Observatory to seek traces of antimatter used as an alien power source. [Korpela et al. \(2015\)](#) simulate the observational signature of giant mirrors put into orbit to illuminate the dark side of a planet. However, the indicator that has attracted the most attention and has been more actively pursued is the concept of Dyson spheres ([Dyson 1960](#)), consisting of astroengineering-scale artificial structures hypothetically employed to harvest power from the parent star. These spheres and other observationally equivalent megastructures would produce occultations of stellar light and excess infrared emission. The most extensive systematic search for this indicator is the  $\hat{G}$  survey (see [Wright et al. 2014b](#); [Wright et al. 2014a](#); [Griffith et al. 2015](#); [Wright et al. 2016](#)).

The main problem with all of the indicators mentioned above is that they would be produced by civilizations with extremely advanced technologies and all of the underlying uncertainties in this uncharted territory increase significantly as we move further away from our own experience. Philosophical and technical questions like what are their motivations, would anyone care

to build a megastructure if they had already developed nuclear fusion or do such advanced species even exist, become more frequent and difficult to answer. For that reason, it is of great interest to develop technomarkers closer to our own technological level. Radio emissions constitute the only such indicator that has been actively explored thus far. However, emissions comparable to ours would be virtually undetectable against the background at interstellar distances unless they were specifically targeted in our direction. In fact, all SETI (Search for Extraterrestrial Intelligence) surveys for radio signals have turned out empty. The current state of non-detection should not be viewed as evidence of ETI absence but as a measure of the enormous difficulties involved in the task ([Editorial 2009](#)). Rather than discouraged, radio SETI efforts have been augmented with other currently ongoing projects (Breakthrough Listen, Allen Telescope Array and SERENDIP, see e.g. [Enriquez et al. 2017](#); [Harp et al. 2016](#); [Chen-namangalam et al. 2017](#) and references therein), in line with the philosophy that a small effort is worthwhile, given the tremendous implications of a potential success.

This paper examines a novel technomarker, the Clarke exobelt (hereafter CEB), for hypothetical civilizations at our current level of technological development (at least in terms of space engineering) but making a heavier use of their planetary space environment. We shall refer to this as a “moderately advanced civilization”, to distinguish from the much more advanced engineering capabilities required for the other indicators mentioned above. The CEB is formed by all objects, including functioning devices and space junk, in geostationary and geosynchronous orbits around a planet. The following sections show the results of numerical simulations demonstrating that, under certain not too implausible circumstances, a CEB would be detectable with currently existing observational means. For some planets, we might have a previous knowledge of the geostationary altitude (see section 3.2). Since nature has no particular preference for this orbit, the mere detection of a population of objects at precisely the CEB altitude would be extremely suggestive of an artificial origin.

## 2. THE CLARKE EXOBELT

Artificial satellites in geostationary and geosynchronous orbits are useful to us for a number of purposes, including telecommunications, surveillance, wild-fire control, geolocation, espionage, wildlife tracking as well as other scientific studies and civil or military applications. The geostationary orbit, often named after Clarke, who explored its practical usefulness for commu-

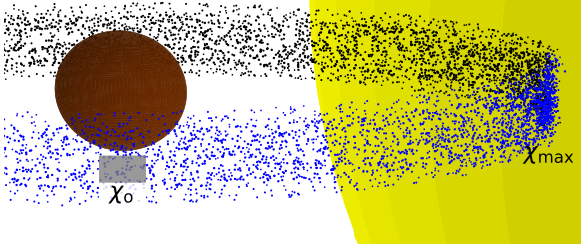


**Figure 1.** Illustrative sketch of a planet with a CEB transiting its parent star. The size and surface density of the individual objects has been exaggerated for better visualization. The face-on opacity  $\chi_o$  (see text for definition) is 0.2 in this case. The edge opacity  $\chi_{\max}$  reaches its maximum possible value of 1.

nication purposes (Clarke 1945), is specially interesting because satellites placed there will remain static as seen from the ground reference frame. However, the available space in that orbit is limited. A moderately advanced civilization might eventually populate it with a relatively high density of objects, making it advisable (cheaper in a supply-and-demand sense) to use geosynchronous orbits when possible for those satellites whose requirements are less strict and allow for some degree of movement along the North-South direction on the sky. Over time, one might expect that societal needs would eventually drive an increase of object density in a band around the geostationary orbit, forming a CEB.

Figure 1 shows a sketch of a transiting exoplanet with a CEB for illustration. The size of individual objects and the belt opacity have been exaggerated<sup>1</sup> in the figure for visibility. The face-on opacity  $\chi_o$  (the opacity of a small surface element when viewed from a perpendicular direction) is 0.2 in this example. The line-of-sight (hereafter l.o.s.) opacity increases as we move away from the center, reaching a maximum value  $\chi_{\max}$  at the edge.

The CEB models presented here are characterized by the following parameters (see Fig 2, upper panel): radius ( $r_C$ ), width ( $w$ ), face-on opacity ( $\chi_o$ ) and inclination of the equatorial plane with respect to the plane of the sky ( $i$ ). A CEB seen edge-on would have  $i = 90^\circ$ . For simplicity, the belt has well-defined sharp borders. It is modeled as a continuous surface, discretized in narrow rectangles (surface elements), as seen in Fig 2. Also for simplicity, the surface is perfectly cylindrical and has zero geometrical thickness. This implies that the model does not consider objects with eccentric orbits and all objects are assumed to have exactly the same orbital

altitude. These approximations are in good agreement with Earth’s current satellite population. According to publicly available data (see Section 3.1 below), the vast majority of geosynchronous satellites have nearly circular orbits (less than 2% have eccentricities above 0.01). The spread in altitude is of  $\simeq 150$  m, only a few parts per million (ppm) of the belt radius.

The belt opacity ( $\chi_o$ ) is defined as the fraction of light in our l.o.s. that is blocked by a surface element (the vertical rectangles in Fig 2). It is a parameterization of the surface density and size of objects on the belt. If a surface element is tilted with respect to our l.o.s., we would see a higher opacity:

$$\chi = \chi_o \sec(\phi) \csc(i). \quad (1)$$

The width parameter  $w$  is related to the maximum orbital inclination  $\gamma$  of geosynchronous satellites  $w = r_C \sin(\gamma)$ . The current industry standard<sup>2</sup> defines a protected geosynchronous region delimited by  $\gamma = 15^\circ$ . According to publicly available databases (see Section 3.1 below), 97% of currently active geosynchronous satellites have orbital inclinations in this range. Taking this value as a starting point, we shall explore simulations with  $\gamma$  between 15 and  $30^\circ$ .

In order to determine the imprint of a CEB on the light curve of the star, we need to calculate the amount of light blocked by the system at each point as it moves across the stellar disk. Taking the  $x$ -axis as the direction of the planet motion on the sky, Fig 2 (lower panel) plots the effective area  $\alpha(x)$ , defined as the geometrical area of the system multiplied by its opacity:

$$d\alpha(x) = y(x)\chi(x)dx, \quad (2)$$

(where  $y$  is the projected size of the system in the direction perpendicular to  $x$  on the sky). The upper and lower panels in Fig 2 share the same abscissae and may be directly compared. The belt opacity varies as indicated by the dashed curve. It has a minimum value  $\chi_o$  at  $x = 0$ , where the belt orientation is most perpendicular to the l.o.s., and increases as the inverse of the cosine of the surface element angle  $\phi$ . The surface elements are represented in the upper panel. They are shown very coarsely for visualization but the actual numerical model used for the calculations has a much finer discretization. For each interval  $dx$ , the code computes the projected area, its opacity and the amount of overlap between the front side and the far side of the belt.

<sup>1</sup> in comparison with the simulations presented in this paper

<sup>2</sup> See, e.g., the Inter-Agency Space Debris Coordination Committee guidelines at <http://www.unoosa.org/documents/pdf/spacelaw/sd/IADC-2002-01-IADC-Space-Debris-Guidelines-Revision1.pdf>

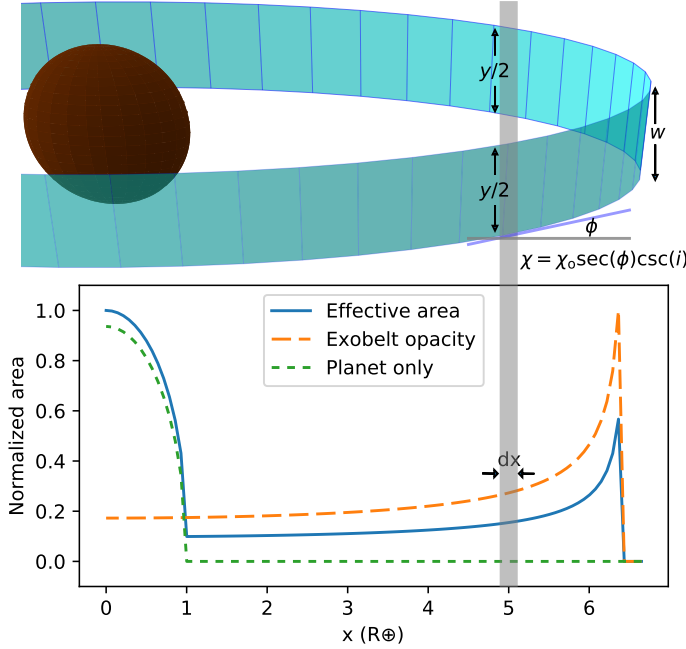


**Figure 2.** Upper panel: Numerical model of a CEB. The azimuth discretization is deliberately coarse for better visualization. The actual calculations have a much finer discretization. See text for symbol definitions. Lower panel: Solid blue line: Effective area  $\alpha(x)$  presented by the entire system as a function of  $x$ . Dashed orange line: Opacity  $\chi$  of the belt in the observer direction, normalized to its maximum value.  $\chi_o$  has been set to 0.03 for an adequate visualization of the belt contribution in this figure (it is much lower in the simulations shown in the figures below). Dashed green line: Same as the solid blue line if the planet had no CEB. Both panels share the same abscissae to allow for a direct comparison.

If there is overlap (as for values of  $x > 5.5$  in the figure), their opacities are added. Since we are working in the  $\chi_o \ll 1$  regime, all the results in this paper will scale with  $\chi_o$ .

### 3. SIMULATIONS

#### 3.1. Earth's belt

Let us first consider the Earth-Sun system as seen from another star. At the present time, we have too few satellites and debris to be detectable at interstellar distances with the technique proposed here. It is difficult to determine with precision the amount of objects in our Clarke belt. Publicly available databases are incomplete and do not consider classified satellites, dead or decommissioned devices, space junk, etc. Nevertheless, it is still insightful to calculate a rough order-of-magnitude estimate of our current  $\chi_o$ .

A particularly useful database is the compilation of data from public sources made by the Union of Con-

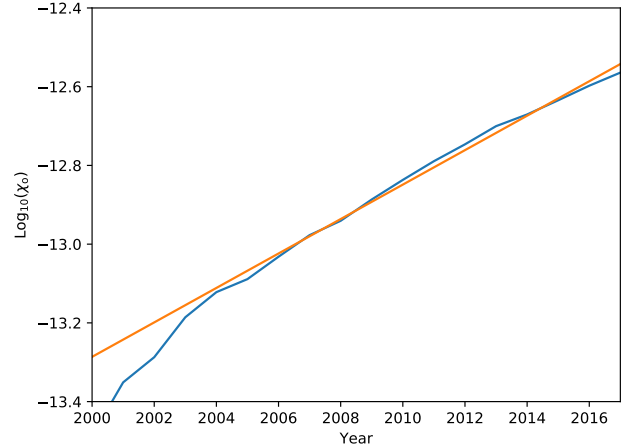


**Figure 3.** Blue: Variation of the  $\chi_o$  parameter for the Clarke belt of humanity over the last decades (notice that the ordinate axis is logarithmic), assuming a typical object radius of 1 m and using public satellite data. Orange: Fit to an exponential increase.

cerned Scientists (UCS)<sup>3</sup>. Currently, the list contains parameters for 1738 satellites, of which approximately one third are in geostationary or geosynchronous orbits. Assuming a typical radius of 1 m, we have that  $\chi_o \simeq 3 \times 10^{-13}$ .

In order to become visible from nearby stars with our current observational capabilities, the Clarke belt of our planet would need to be about  $\chi_o \sim 10^{-4}$  (see below). Therefore, it is reasonable to assume that we are probably orders of magnitude below the detection threshold of any possible observer. However, our belt is becoming increasingly populated. Figure 3 shows that the Earth belt opacity  $\chi_o$  has been growing exponentially over the last 15 years. If this trend is extrapolated into the future, we would reach the “observable” threshold ( $\sim 10^{-4}$ ) around the year 2200.

Obviously, this extrapolation should not be viewed as a prediction. There is no reason to assume that the current exponential growth will be sustained for another 200 years. It might slow down if the demand for orbital devices were to decline, or it could accelerate if new technologies were developed that either require or facilitate the addition of more devices. In this respect it is worth pointing out another Clarke invention: a “space elevator” system would tremendously facilitate access to geostationary orbit, which is a natural place to stop, and

<sup>3</sup> The UCS database with references to the original sources is available online at [http://www.ucsusa.org/satellite\\_database](http://www.ucsusa.org/satellite_database). The calculations presented in this paper make use of release 9-1-17.

would likely speed up the rate of  $\chi_o$  growth. In summary, the 2200 date is not even a rough guess of when humanity will reach detectability threshold but rather an indication that this outcome is a reasonable expectation for the near future, given current trends.

Let us consider the appearance of our system, as seen from another star, in a hypothetical future with a more cluttered Clarke belt. Figure 4 depicts the light curve of Earth with a  $\chi_o = 10^{-3}$  belt, transiting the Sun as viewed from a distance of 10 light-years. Random noise is computed assuming a perfect 10 m aperture telescope doing white-light photometry with 60 s exposures. This simulation assumes a black-body spectral distribution of the stellar radiation, filtered with the spectral response of the Kepler mission<sup>4</sup>. All of the light curves computed in this paper have noise dominated by photon detection statistics. For simplicity, the code assumes zero impact parameter in all transits and neglects limb-darkening. The events marked as CEB<sub>1</sub> and CEB<sub>2</sub> in the plot (see figure insets for details) are produced by the belt. Both events are clearly above the noise, at the ppm level. For a sake of reference, consider that the Kepler mission has a photometric precision of  $\sim 10$  ppm. Therefore, in this case study, the belt would be detectable using current technology. It is not far from the capabilities of existing planet hunting missions.

### 3.2. Other planets

The radius  $r_C$  of a CEB is a function of the planet mass but also its rotation, according to the expression:

$$r^3 = \frac{G}{4\pi^2} MT^2 \quad (3)$$

where  $G$  is the universal gravitational constant,  $M$  is the mass of the planet and  $T$  is the rotation period. An interesting insight from the above formula is that  $r_C$  depends very weakly on  $M$ , only as a power of  $1/3$ . This is very fortunate because, for many transiting exoplanets, we have no radial velocity measurements and therefore the mass is uncertain. However, we do have an accurate determination of the size and our uncertainty in the planet density translates into a much lower uncertainty in the CEB radius  $r_C$ . For instance, Venus, Earth and Mars have a density spread of 37% (Mercury is peculiar, with an anomalously high density more characteristic of a planetary core). If we take this as the typical uncertainty on Earth-like planet densities, the associated uncertainty on  $r_C$  would be 11%. This discussion does not apply to super-Earths, which are likely to have considerably higher densities.

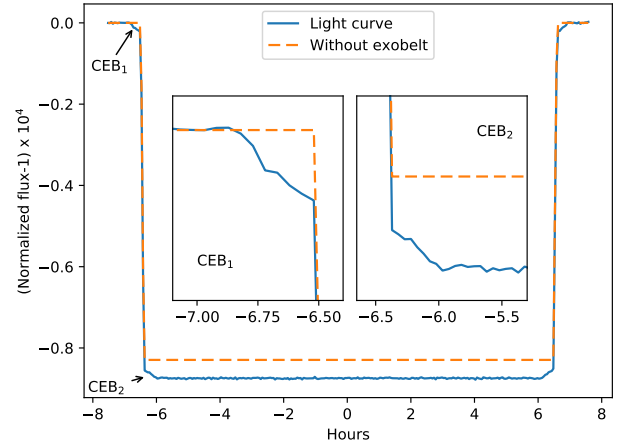


**Figure 4.** Synthetic light curve computed for an Earth-like planet transiting a Sun-like star at a distance of 10 light-years. The planet has a CEB of  $\chi_o = 10^{-3}$ ,  $\gamma = 20^\circ$  and  $i = 70^\circ$ . The arrows indicate the positions of the belt transits during the ingress (they have symmetric counterparts during egress). CEB<sub>1</sub> marks the light-curve drop from the CEB exterior ingress until the planet exterior ingress. From CEB<sub>1</sub> to CEB<sub>2</sub> the planet moves into the stellar disk. CEB<sub>2</sub> marks the ingress of the trailing half of the CEB behind the planet. The inset plots show close ups of both CEB<sub>1</sub> and CEB<sub>2</sub> events.

The rotation period  $T$  may be straightforward, very difficult or impossible to estimate, depending on the situation. Berdyugina & Kuhn (2017) examined the observational requirements to produce time-dependent spectroscopic maps of a planet surface. For the case of Proxima b they concluded that a low scattered light telescope with an aperture of more than 12 m may be able to accomplish this task. Surface inhomogeneities would imprint a periodic spectral modulation that would reveal its rotation period with very high accuracy. If a planet exhibits surface albedo variations on a global scale, it would be possible to determine its rotation period more easily, and therefore at greater distances, than via spectroscopy. Kawahara & Fujii (2010) showed that future space missions may produce surface maps of planets up to 5 pc away. In any case, both photometric and spectroscopic rotation measurements would require next-generation instrumentation and would only be feasible for systems relatively close to us.

The planet rotation period might be straightforwardly obtained if it is tidally locked, which is probably very frequent for the most interesting exoplanet candidates. Earth seems to be rather peculiar in this regard. According to some models (Barnes 2017), without atmosphere, moon and assuming constant tidal properties, it would

<sup>4</sup> <https://keplergo.arc.nasa.gov/CalibrationResponse.shtml>

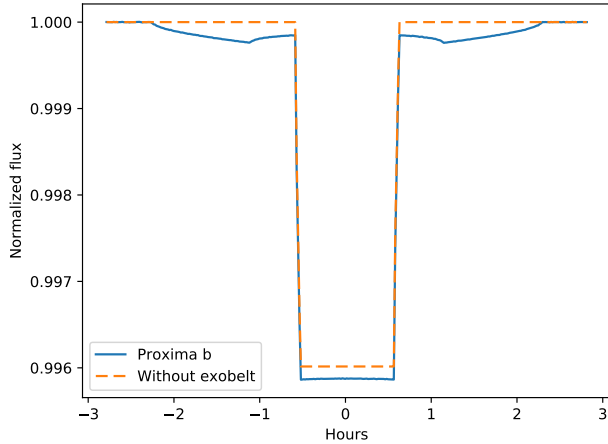


**Figure 5.** Synthetic light curve computed for Proxima b with a CEB having  $\chi_o = 5 \times 10^{-5}$ ,  $\gamma = 20^\circ$ ,  $i = 80^\circ$ .

have already synchronized its rotation with the orbital motion around the Sun, resulting in days of the same duration as a year. However, tidal locking in the habitable zone (Kasting et al. 1993; Kopparapu 2013) may be very common (however, counterarguments exist for planets with dense atmospheres, e.g. Auclair-Desrotour et al. 2017) and its frequency should increase from G to K and M type stars. The smaller stars (types K and M) are by far the most abundant in the galaxy and, furthermore, exoplanet detection is observationally easier there. Therefore, they have become the prime candidates for planet search projects and, lacking better criteria, possibly the most interesting targets for the search of indicators such as the one explored in this paper. According to Barnes (2017), half of the Kepler planet candidates and the vast majority of the ones expected to be discovered by TESS become tidally locked in less than 1 Gyr. Therefore, it seems plausible that we might be able to obtain a good estimate of the CEB radius for a potentially interesting candidate.

Let us now consider the light curve, starting with the closest exoplanet in habitable zone, Proxima b, as a particularly relevant reference. Figure 5 shows the light curve of a transit with  $\chi_o = 5 \times 10^{-5}$ ,  $\gamma = 20^\circ$  and  $i = 80^\circ$  observed with a 10 m telescope in near-infrared J-band photometry (using the standard Mauna Kea filter definition). The star and planet data employed are listed in Table 1 and have been obtained from Anglada-Escudé et al. (2016) and Bixel & Apai (2017). As the figure shows, we could easily detect the presence of a CEB with  $\chi_o$  lower than  $10^{-4}$ .

Another system of great interest is TRAPPIST-1, with seven confirmed rocky planets in habitable zone or

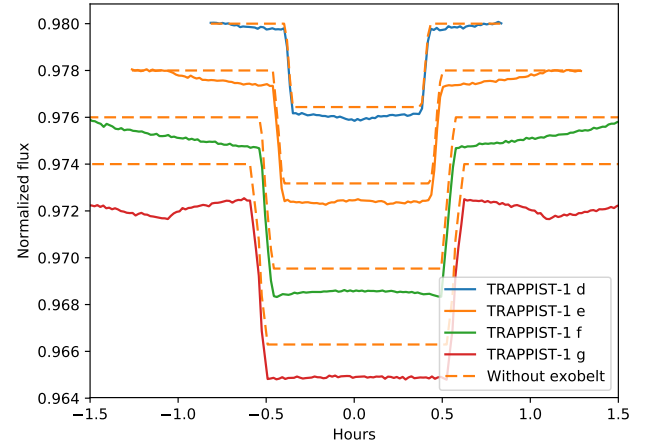


**Figure 6.** Synthetic light curve computed for TRAPPIST-1 planets with a CEB having  $\chi_o = 5 \times 10^{-4}$ ,  $\gamma = 20^\circ$ ,  $i = 80^\circ$ . The light curves for the various planets have been shifted vertically to show them all without overlap.

very close to it, allowing for an accurate determination of their masses and almost certainly tidally locked. The most likely habitable planets in the TRAPPIST-1 system are d to g, which span a range of masses, distances and periods listed in Table 1. Data for the star and planets have been taken from Van Grootel et al. (2017), Wang et al. (2017) and Delrez et al. (2018). The synthetic light curves of all of these planets with a CEB are shown in Fig 6. The parameters chosen for the calculations are  $\chi_o = 5 \times 10^{-4}$ ,  $\gamma = 15^\circ$  and  $i = 80^\circ$ . Reducing  $\chi_o$  to  $10^{-4}$  would still result in observable signatures for all except the innermost planet TRAPPIST-1 d.

### 3.3. Rings

Wright et al. (2016) explored the possible confounding natural factors in the general context of artificial constructions around stars or planets, including rings. At first sight, the imprint of a CEB on the light curve is similar to that of a ring system. A smaller dip in intensity, marked as CEB<sub>1</sub> in Fig 4, appears just before the planet exterior ingress (the intensity drop caused by the planet moving into the stellar disk). Afterwards, another dip (marked as CEB<sub>2</sub> in Fig 4) appears just after the interior ingress (the endpoint of the intensity drop). This pattern of dips just before and after the planet ingress is also produced by ring systems (Arnold & Schneider 2004). The question then is, can we infer from this signature the presence of extraterrestrial intelligence? Let us assume that we detect a promising candidate planet, meeting some basic criteria (rocky and at a suitable temperate distance from its parent star) with

**Table 1.** Planet parameters employed for light-curve calculations. In parentheses are the actual values published in the references, when different or highly uncertain.

Planet	Mass	Radius	Orbit	Rotation	Distance	Star radius	Star luminosity	T <sub>eff</sub>
	(M <sub>⊕</sub> )	(R <sub>⊕</sub> )	(UA)	(days)	(ly)	(R <sub>⊙</sub> )	(10 <sup>-4</sup> × L <sub>⊙</sub> )	(K)
Proxima b	2.6 (>1.3)	1.0 (0.8-1.5)	0.0485	11.2	4.22	0.14	15	3050
TRAPPIST-1 d	0.33	0.78	0.022	4.0	39.6	0.12	5.2	2516
TRAPPIST-1 e	0.60	0.91	0.029	6.1	39.6	0.12	5.2	2516
TRAPPIST-1 f	0.70	1.05	0.038	9.2	39.6	0.12	5.2	2516
TRAPPIST-1 g	1.30	1.15	0.047	12.3	39.6	0.12	5.2	2516

dips before and after planet ingress corresponding to a distance  $x$  from its center.

The first question is whether planets of this kind are likely to host ring systems. In principle, dynamical studies suggest that rings might indeed exist around temperate planets (Schlichting & Chang 2011) and remain stable on Gyr time-scales. However, there are also indications that rings might occur predominantly in planets beyond the ice line and would be less frequent in the habitable zone rocky planets that are the main target of current SETI. The search for exoplanets, which is biased towards inner planets with shorter orbital periods, has not yet found any proper ring system in the more than 3,700 planets discovered thus far. The only exception, 1SWASP J140747.93394542.6 (Mamajek et al. 2012), has a disk that is much larger than the planet’s Roche lobe and should probably be considered a transient protosatellite moon rather than a stable ring system (Hatchett et al. 2018). Furthermore, in our own Solar System we find that all the planets beyond the ice line have rings, in addition to other smaller bodies such as Haumea, Chariklo and, possibly, Chiron. In contrast, none of the inner Solar System bodies have rings. Hedman (2015) proposed that this could be explained assuming that the ice-rich material becomes weak at low temperatures ( $\sim 70$  K), facilitating fragmentation and formation of rings.

We still have very little understanding of exoring formation and their probability of occurrence, especially in the habitable zone. Given the considerations discussed above, the observation of CEB-like features in the transit of a candidate planet should be viewed as extremely suggestive. The next obvious question would be whether it has the right orbital altitude.

For most planets, we can determine the CEB radius  $r_C$  directly from their mass and rotation period. Recall that, as discussed above,  $r_C$  is very weakly dependent

on the mass (it goes with the power of  $1/3$ ). This means that, even in the absence of proper mass measurements, the size of an Earth-like planet (which is straightforwardly determined from the transit light curve) is sufficient to constrain  $r_C$  to approximately 11%. Rotation might be measured observationally (although this would be very challenging) or derived trivially if the planet is tidally locked, which may be the case for many interesting candidates. With these considerations in mind, it is very likely that we would have a robust determination of  $r_C$  for our planet candidate. If it happened to exhibit the dips at the right distance ( $x = r_C$ ), it would be a very strong indication of an artificial origin. Geostationary orbits are very interesting for a society but are not preferred by any known natural process.

Let us now examine the issue of whether detailed extensive observations could resolve the ambiguity between rings and a CEB. These two structures have a different intrinsic geometry. Both are extremely thin and flat but in different (perpendicular) directions. Rings are extended in the radial direction and thin in inclination. CEBs, on the other hand, are thin in the radial direction and extended in inclination. With some straightforward modifications, the code used for the calculations presented in the previous sections may be adapted to compute a simple ring system in the same conditions, allowing for a detailed comparison of both scenarios. Note, however, that a large ring system might have a more complex geometry with radial variations of opacity, such as the gaps in Saturn’s rings, which would not be captured by this simple model.

As a result of their different geometry, the effective area curve  $\alpha(x)$  produced by rings and CEBs are markedly different. A comparison is plotted in Fig 7. The figure illustrates a particular configuration but the overall conclusion is rather general and easily understood from the geometry of the problem. The CEB has

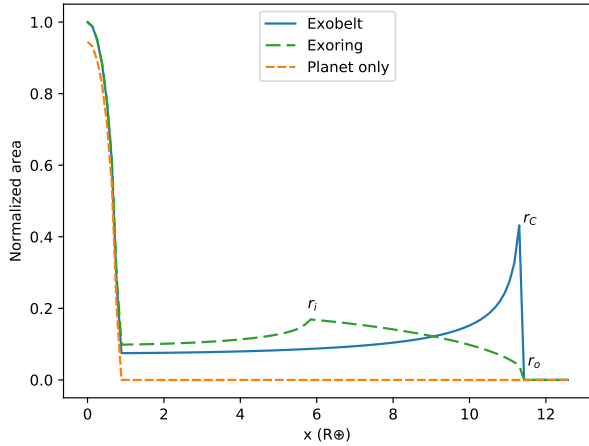


**Figure 7.** Effective area  $\alpha(x)$  presented by a planet with CEB (solid blue), a planet with rings (dashed green) and an isolated planet (dashed orange). Notice the overall concave shape of the CEB curve as opposed to the ring, which changes from concave to convex from left to right at  $r_i$ . This simulation has  $i = 80^\circ$  and  $\gamma = 20^\circ$ . The ring has inner and outer radii  $r_i = r_C/2$  and  $r_o = r_C$ .

its maximum opacity at the very edge but its projected area does not change significantly with  $x$ . The ring, on the other hand, has an approximately constant opacity and its area increases gradually from the outer to the inner radius.

The differences in  $\alpha(x)$  translate into subtle but measurable differences in the light curve. This is shown in Fig 8. For a CEB, the first dip (CEB<sub>1</sub>) is always concave, while the second one (CEB<sub>2</sub>) is always convex. This is a direct result of the variation of  $\chi$  in the transit direction which, as explained above, goes with the secant of  $\phi$ . The ring, on the other hand, switches from convex to concave in both dips. This behavior is a consequence of the variation in the ring projected area, from edge to center (see Fig 7). For both, CEB and ring system, the light curve convexity reflects the convexity of  $\alpha(x)$ , which is constant for the CEB (always concave) but switches sign for the ring system, going from convex at the outer radius to concave at the inner radius.

Another difference is that the ring system has a flat start and end to the dip. The transition between a flat light curve and the dip is smooth. The CEB, on the other hand, has a maximum slope at the start and the end. There is a marked discontinuity in the derivative of the light curve at the endpoints. This is caused by the fact that the CEB has its maximum opacity at the edge and then drops abruptly to zero. The ring, on the other

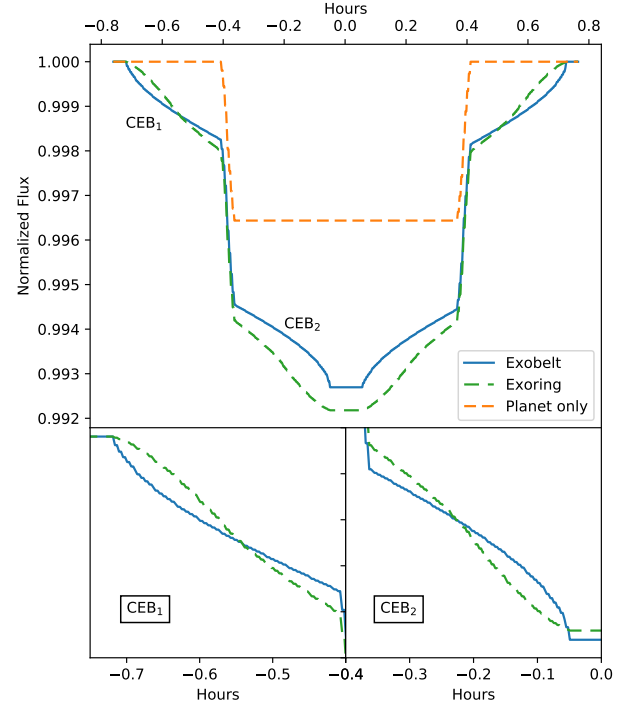


**Figure 8.** Synthetic light curves corresponding to the simulation of Fig 7. The upper panel shows the entire transit. The lower panels show a close-up of the regions CEB<sub>1</sub> and CEB<sub>2</sub>. The green dashed line in CEB<sub>2</sub> has been shifted vertically to facilitate visual comparison.

hand, starts with zero area at the outer radius and then increases gradually as the ingress progresses (Fig 7).

#### 4. CONCLUSIONS

One of the main conceptual difficulties in the SETI effort is our complete lack of knowledge on the motivations or interests of other civilizations. We are forced to guess what other peoples, with whom we share absolutely no common cultural background, are trying to build or accomplish. For instance, our searches are focused on planets but perhaps civilizations with highly advanced capabilities might have decided to move away from the perils of stars and planets and dwell instead in the dark safety of interstellar space, connected to their parent system only to retrieve minerals and fusion fuel. This is simply an example of the many uncertainties and unconscious biases involved in the complex SETI guesswork. Therefore, it is important to develop technomarkers with which to expand the search to include civilizations at a level of technological development as close as possible to our own.

The indicator analyzed here is a step in that direction. A CEB does not require of any technology that we do

not have, only a more extensive use of orbital space. Perhaps their civilization is older than ours and has had more time to populate it. Or perhaps it has been driven by a stronger push for space devices, for reasons that we could only speculate about.

The numerical model has some basic simplifying assumptions. In reality, there would be more devices in other orbits around the planet. The belt might have some thickness due to slightly different orbital altitudes and some fraction of geosynchronous satellites may have eccentric orbits. However, small deviations from this idealized model will not have a significant effect on the main results. There is always the possibility that an ETI might develop a completely different approach in populating their CEB but the goal of this paper is to explore the consequences of a direct extrapolation of our current trends.

The simulations presented here show that CEBs may in some situations be detectable with existing instrumentation. The best candidates are planets around red dwarfs in tidal locking, in line with the optimal conditions for habitable exoplanet search. An initial difficulty would be how to distinguish between a CEB and a ring system. However, once a candidate has been identified, detailed follow-up observations may resolve this ambiguity from the shape of the light curve. In any case, the detection of a dense belt of objects at the distance of geostationary orbit would be a very strong evidence for the presence of ETI, especially considering that rings around habitable rocky planets are probably rather uncommon.

While the similarity between a CEB and a ring system poses an initial difficulty, it also opens new opportuni-

ties. Existing interest in the physics of exorings and exomoons means that large efforts will be devoted in future photometric missions to examine rocky planet transits for evidence of such objects. This paper shows how future positive detections of orbital material may be further scrutinized for evidence of CEBs, making the search for moderately advanced technologies “piggyback” on such missions.

The total mass of the entire belt for all the cases considered here (Earth, Proxima b and TRAPPIST-1 planets d to g) is between  $10^{12}$  and  $10^{14}$  kg, assuming  $\chi_o=5\times 10^{-4}$ ,  $\gamma=20^\circ$  with average object radius and mass of 1 m and 100 kg. This range is between the mass of a comet and that of a mountain. It is not an unreasonable requirement for a moderately advanced civilization.

One exciting perspective about a CEB discovery is that it would most likely point to the presence of an active civilization. Other technomarkers, such as Dyson spheres or swarms, could have been built by species that disappeared, moved away or became extinct long ago. A crowded CEB, on the other hand, requires active maintenance to keep objects in proper orbits and away from collisions with other nearby objects. A dynamical study of the relevant timescales is beyond the scope of this paper but for our current satellites, such scales are typically of the order of decades.

As with any other technomarkers, the search for CEBs is a long shot. We have no idea if they exist or how likely they are to occur. However, given that candidate identification is based on the same light curve observations that are currently demanded in the search for habitable exoplanets, it does not require of any additional effort, at least initially, other than being alert for possible detections.

## REFERENCES

- Angel, R., Codona, J. L., Hinz, P., & Close, L. 2006, in Proc. SPIE, Vol. 6267, Society of Photo-Optical Instrumentation Engineers (SPIE) Conference Series, 62672A
- Anglada-Escudé, G., Amado, P. J., Barnes, J., et al. 2016, *Nature*, 536, 437
- Arnold, L., & Schneider, J. 2004, *A&A*, 420, 1153
- Astropy Collaboration, Robitaille, T. P., Tollerud, E. J., et al. 2013, *A&A*, 558, A33
- Auclair-Desrotour, P., Laskar, J., Mathis, S., & Correia, A. C. M. 2017, *A&A*, 603, A108
- Barnes, R. 2017, *Celestial Mechanics and Dynamical Astronomy*, 129, 509
- Berdyugina, S. V., & Kuhn, J. R. 2017, ArXiv e-prints, arXiv:1711.00185
- Bixel, A., & Apai, D. 2017, *ApJL*, 836, L31
- Chennamangalam, J., MacMahon, D., Cobb, J., et al. 2017, *ApJS*, 228, 21
- Clarke, A. C. 1945, *Wireless World*, 55, 305
- Delrez, L., Gillon, M., Triaud, A. H. M. J., et al. 2018, ArXiv e-prints, arXiv:1801.02554
- Dyson, F. J. 1960, *Science*, 131, 1667
- Editorial. 2009, *Nature*, 461, 316
- Enriquez, J. E., Siemion, A., Foster, G., et al. 2017, *ApJ*, 849, 104
- Forgan, D. H., & Elvis, M. 2011, *International Journal of Astrobiology*, 10, 307

- Grenfell, J. L. 2017, ArXiv e-prints, arXiv:1710.03976
- Griffith, R. L., Wright, J. T., Maldonado, J., et al. 2015, *ApJS*, 217, 25
- Harp, G. R., Richards, J., Tarter, J. C., et al. 2016, *AJ*, 152, 181
- Harris, M. J. 2002, *Journal of the British Interplanetary Society*, 55, 383
- Hatchett, W. T., Barnes, J. W., Ahlers, J. P., MacKenzie, S. M., & Hedman, M. M. 2018, *NewA*, 60, 88
- Hecht, J. 2016, *Nature*, 530, 272
- Hedman, M. M. 2015, *ApJL*, 801, L33
- Hunter, J. D. 2007, *Computing In Science & Engineering*, 9, 90
- Kasting, J. F., Whitmire, D. P., & Reynolds, R. T. 1993, *Icarus*, 101, 108
- Kawahara, H., & Fujii, Y. 2010, *ApJ*, 720, 1333
- Kopparapu, R. K. 2013, *ApJL*, 767, L8
- Korpela, E. J., Sallmen, S. M., & Leystra Greene, D. 2015, *ApJ*, 809, 139
- Lingam, M., & Loeb, A. 2017, *ApJL*, 837, L23
- Mamajek, E. E., Quillen, A. C., Pecaute, M. J., et al. 2012, *The Astronomical Journal*, 143, 72.  
<http://stacks.iop.org/1538-3881/143/i=3/a=72>
- Pérez, F., & Granger, B. E. 2007, *Computing in Science and Engineering*, 9, 21. <http://ipython.org>
- Quanz, S. P. 2015, *European Planetary Science Congress*, 10, EPSC2015
- Schlichting, H. E., & Chang, P. 2011, *ApJ*, 734, 117
- Schneider, J., Léger, A., Fridlund, M., et al. 2010, *Astrobiology*, 10, 121
- Schwieterman, E. W., Kiang, N. Y., Parenteau, M. N., et al. 2017, ArXiv e-prints, arXiv:1705.05791
- Seager, S., Deming, D., & Valenti, J. A. 2009, *Astrophysics and Space Science Proceedings*, 10, 123
- Van Der Walt, S., Colbert, S. C., & Varoquaux, G. 2011, *Computing in Science & Engineering*, 13, 22
- Van Grootel, V., Fernandes, C. S., Gillon, M., et al. 2017, ArXiv e-prints, arXiv:1712.01911
- Wang, S., Wu, D.-H., Barclay, T., & Laughlin, G. P. 2017, ArXiv e-prints, arXiv:1704.04290
- Wright, J. T., Cartier, K. M. S., Zhao, M., Jontof-Hutter, D., & Ford, E. B. 2016, *ApJ*, 816, 17
- Wright, J. T., Griffith, R. L., Sigurdsson, S., Povich, M. S., & Mullan, B. 2014a, *ApJ*, 792, 27
- Wright, J. T., Mullan, B., Sigurdsson, S., & Povich, M. S. 2014b, *ApJ*, 792, 26
- Wright, S. A., Larkin, J. E., Moore, A. M., et al. 2014c, in *Proc. SPIE*, Vol. 9147, *Ground-based and Airborne Instrumentation for Astronomy V*, 91479S

The author gratefully acknowledges financial support from the Spanish Ministry of Economy and Competitiveness through project AYA2014-60476-P. This research has made use of NASA's Astrophysics Data System Bibliographic Services. The Python Matplotlib (Hunter 2007), Astropy (Astropy Collaboration et al. 2013), Scipy (<http://www.scipy.org>), Numpy (Van Der Walt et al. 2011) and iPython (Pérez & Granger 2007) modules have been used to generate the figures and some calculations for this paper. The author thanks the anonymous referee for valuable comments that helped improve an earlier manuscript.